Physical Modelling in Geotechnics

High speed observation on damage process of embankments during earthquakes in a centrifugal acceleration field

R. Ibuki, T. Doi & J. Izawa
Soil Dynamics and Earthquake Engineering Laboratory, Railway Technical Research Institute, Tokyo, Japan

K. Uemura & S. Sreng
R&D Center, Nippon Koei, Co., Ltd., Ibaraki, Japan

ABSTRACT: In this study, we conducted a centrifuge shake table test of a relatively stiff embankment to evaluate its damage process during earthquakes. To observe seismic behavior of the embankment, digital images of the embankment were taken at intervals of 0.01seconds under the centrifugal acceleration of 50G (0.5 seconds in prototype) with the high-speed digital camera. The camera was fixed to the shake table for removing camera shake. Using the digital images, strain distributions inside the embankment were calculated with the particle image velocimetry (PIV) analysis. Accordingly, we could clearly observe progress of strain inside the embankment up to sliding failure as follows, (i) the embankment tended to compress with shaking; (ii) the shear strain began to concentrate at the particular part of slope; (iii) the shear strain progressed into the inside of the embankment; (iv) sliding failure occurred as soon as a sliding plane appeared. We compared the maximum shear strain at the strain concentration part with the shear stress-strain relationship of the embankment material. As a result, we found that a sliding plane appears when the maximum shear strain at the strain concentration part reaches the shear strain at the peak stress of the embankment material.

Keywords: embankment, centrifuge modelling, high-speed camera, PIV, damage process

1 INTRODUCTION

The Newmark's sliding block method (Newmark, 1965) has been often used for seismic design of embankments (e.g., Railway Technical Research Institute, 2012). The Newmark's sliding block method calculates sliding displacement of the soil block after occurrence of a sliding failure. Many studies (e.g., Sarma, 1975; Makdisi and Seed, 1978;) have been carried out to precisely evaluate the seismic performance of embankments. However, some researchers have reported that the Newmark's sliding block method cannot accurately simulate the actual damage state of embankments observed in past large earthquakes (e.g., Fujiwara et al., 2015).

Izawa et al., 2022 conducted a series of the centrifuge shake table tests to observe the damage process of embankments during earthquakes using the PIV analysis (White and Take, 2003). They found that the damage process up to occurrence of sliding failure depends on the slope of embankments. For embankments with a steep slope, the shear strain concentrates near the toe of the slope and causes sliding failure as shown in Figure 1. On the other hand, for embankments with a gentle slope, shaking-down settlement mainly occurs without sliding failure even against severe earthquakes. In addition, they have proposed a performance verification method, which can evaluate the damage process observed in the centrifuge shake table tests. The damage process during earthquakes is not, however, fully clarified during shaking, because in these tests results were observation based on the PIV analysis using digital images taken after shakings. In this study, we attempted to observe the damage process of embankments during earthquakes in the centrifugal acceleration field.

2 OUTLINE OF THE TEST

2.1 Camera setup

Some researchers tried to use a high-speed camera in a centrifugal acceleration field to observe seismic behavior of geotechnical structures for a few decades. For example, Okamura et al., 2001 applied a high-speed camera to measure a displacement of the model caissons and their supporting ground in a centrifugal acceleration of 50G. They installed the camera on the rotation arm of the centrifuge and tracked the target makers set on the model and the control marker set on the glass wall. Ito et al., 2009 developed the rockfall generation system for the centrifuge to capture the trajectory of falling rocks using a high-speed camera in the centrifugal acceleration of 50G. Furthermore, Cilingir et al., 2011 attempted to employ the PIV technique for high-speed camera images obtained from the dynamic centrifuge tests of square

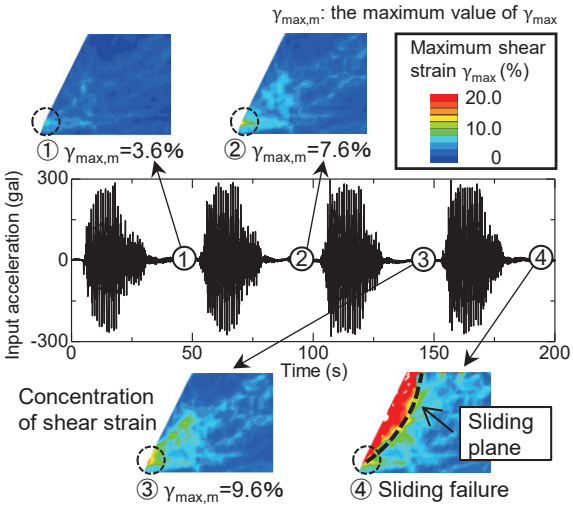

Fig. 1. The damage process up to sliding failure in the case with a steep slope (reconstruction Izawa et al., 2022). $\gamma_{max,m}$ is the maximum value of γ_{max}.

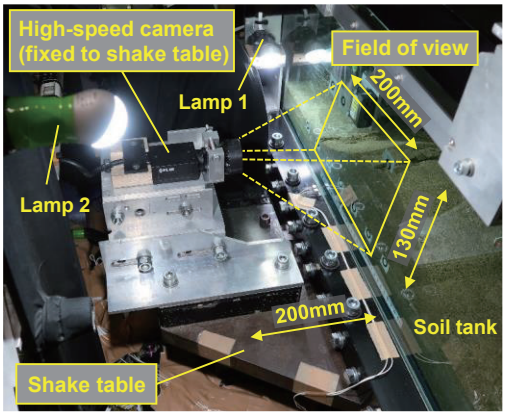

Fig. 2. Location of high-speed

tunnels, but high-speed camera images taken during earthquakes were not shown. Since it is quite difficult to conduct full-scale shake table tests of geotechnical structures, such detailed observation of small models during earthquakes in a centrifugal acceleration field greatly contributes to clarification of a variety of geotechnical earthquake problems. In this study, we tried to obtain high speed digital images of embankments during earthquakes in the centrifugal acceleration of 50G and clarify the damage process of an embankment in detail by the PIV analysis.

The beam type centrifuge with a diameter of 5.2m and the shake table of the Nippon Koei Co. LTD. (Sreng et al., 2015) were used in this study. A high-speed and high-resolution digital camera with global shutter (Teledyne FLIR LLC, The Grasshopper3 GS3-U3-32S4C-C, Frame rate: 121 fps, Resolution: 2048×1536, Sensor type: CMOS) was used, being fixed to the shake table to exclude camera shake as shown in Figure 2. A sensor format of 1/1.8" and a lens with a focal length of 3.5mm were selected in order to sufficiently secure the

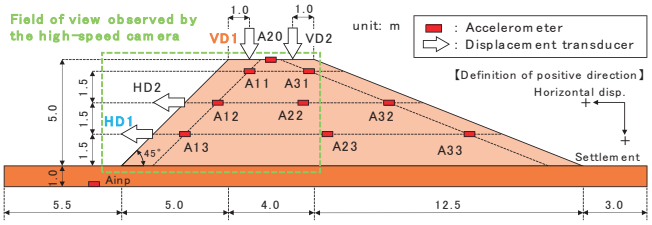

Fig. 3. Schematic view of model embankment.

Table 1. Physical properties of the Edosaki sand.

Soil particle density	: G_s	2.68
Mean grain size	: D_{50}	0.34 mm
Effective grain size	: D_{10}	0.15 mm
Uniformity coefficient	: Uc	2.6
Coefficient of curvature	: $U'c$	1.00
Fine content	: Fc	4.4%
Optimum water content	: w_{opt}	14.6%
Maximum dry density	: ρ_{dmax}	1.707 g/cm^3

Table 2. Physical and Mechanical properties of the Edosaki sand.

Dry density	: ϕ_d	1.622 g/cm^3
Degree of compaction	: D_c	95 %
Compression index	: C_c	0.055
Consolidation yield stress	: P_c	318.1 kPa
Cohesion	: c	8.65 kPa
Internal friction angle	: ϕ	36.4 deg.

field of view with approximately 400mm in width and 300mm in height under the condition of approximately 200mm distance from the soil tank to the camera. In this test, the field of view was set to 200mm in width and 130mm in height due to limitation of saving digital image data in the on-board PC. Two lamps were installed beside and behind the camera to light the field of view equally. The shooting speed was set to be 0.01 seconds in the centrifugal acceleration of 50G, which corresponds to 0.5 seconds in prototype scale. As will be shown later, we could obtain very clear high-resolution images with no distortion and employ the PIV analysis using the images without any calibrations.

2.2 Model setup

Figure 3 shows the schematic view of the model embankment and the sensor arrangement. Slope of the left side embankment was set to be 1:1.0, which is steep enough to induce a sliding failure during shakings, since the purpose of this study is to capture the damage process of embankments leading to sliding failure. The slope of the other side was 1:2.5 so as not to cause a sliding failure. In constructing the model, the embankment was divided into 5 layers with 20mm and compacted each layer to obtain the heigh of 100mm, which corresponds to 5m in prototype scale.

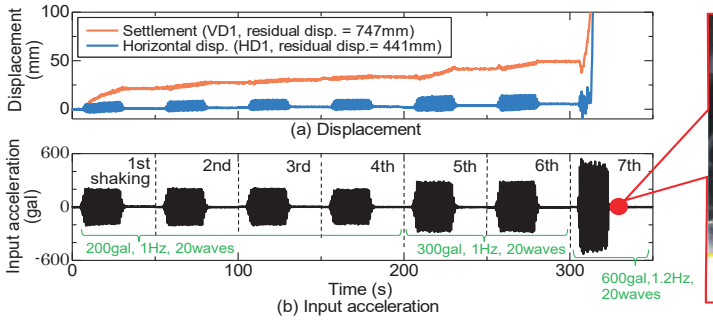

Fig. 4. Time histories of displacement and input acceleration.

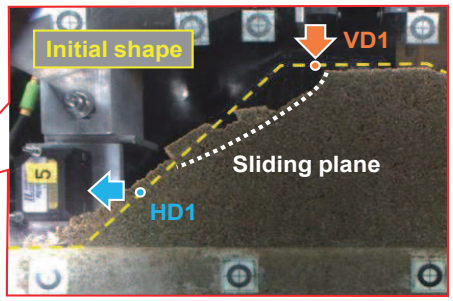

Fig. 5. Image of the embankment model after the 7th shaking.

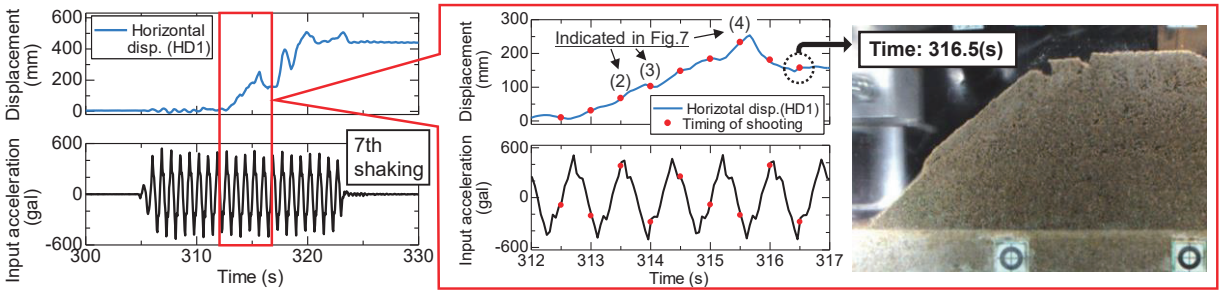

Fig. 6. Magnified view of the time histories of displacement and input acceleration during 7th shaking.

The Edosaki sand was used as the embankment material with a degree of compaction (Dc) of 95%. Tables 1 and 2 summarize the physical and mechanical properties obtained from some laboratory tests, respectively. The natural period of the model before shaking was measured by applying small white noise shaking to the model before main shakings. As a result, the natural period was identified to be 0.104 seconds in prototype.

3 RESULTS AND DISCUSSIONS

Some types of sinusoidal seismic waves were repeatedly applied so that the deformation process until the sliding failure of the embankment could be observed in detail. Figure 4 shows the time histories of the settlement (VD1), horizontal displacement (HD1) and the input acceleration from 1st to 7th shaking.

From 1st to 6th shaking, the settlement at the crown gradually increased without large residual horizontal displacement. In 7th shaking, the horizontal displacement increased rapidly, and the embankment collapsed showing clear sliding plane as shown in Figure 5. Figure 6 shows magnified view of the time histories of the horizontal displacement and the input acceleration at 7th shaking. The red plots in Figure 6 indicate the capturing timing of digital images. Upper part of Figure 7 shows the digital images at 7th shaking step and the distributions of the maximum shear strain (γ_{max}) obtained from the PIV analysis. In the PIV analysis, the digital image taken just before 1st shaking is used as the initial state. The maximum value of γ_{max} is also indicated as $\gamma_{max,m}$ in Figure 7. It is confirmed that shear strain gradually concentrated at the particular part of the slope (we call this part "strain concentration part" hereafter) and progressed into the inside of the embankment during shaking. After that, a sliding plane appeared and the embankment collapsed (Figure 7(4) at 315.5s). Lower part of Figure 7 shows the stress-strain relationship of the Edosaki sand obtained from the monotonic shear loading test with the hollow cylinder torsional shear test apparatus at confining pressure of 50kPa. In this paper, we treat this stress-strain relationship as the relationship between shear stress and maximum shear strain at the strain concentration part in the model embankment. Approximately $\gamma_{max,m}$ of 5.0% occurred before 7th shaking as shown in Figure 7(1) (at 300s), which did not reach the strain at peak stress of the embankment material (7.2%). During the 7th shaking, $\gamma_{max,m}$ at the strain concentration part increased and reached 7.2% between 313.5s and 314.0s. Note that 7.2% is the peak stress indicated lower part of Figure 7. After that, shear strain rapidly increased and finally collapsed while showing the sliding plane as shown in Figure 7(4). This means that an embankment would show sliding failure when the shear strain at the concentration part near slope reaches the strain at peak stress of the embankment material. This damage process is in good agreement with the previous study (Izawa et al., 2022). Furthermore, it is found that the strain concentration part observed during shaking corresponds to that at initial condition as shown in Figure 7 (5). It can be said that the strain begins to concentrate at the edge of the potential sliding plane formed before shaking and progresses along the plane during earthquake. The edge of the plane observed in this test, that is, the strain concentration part, was located

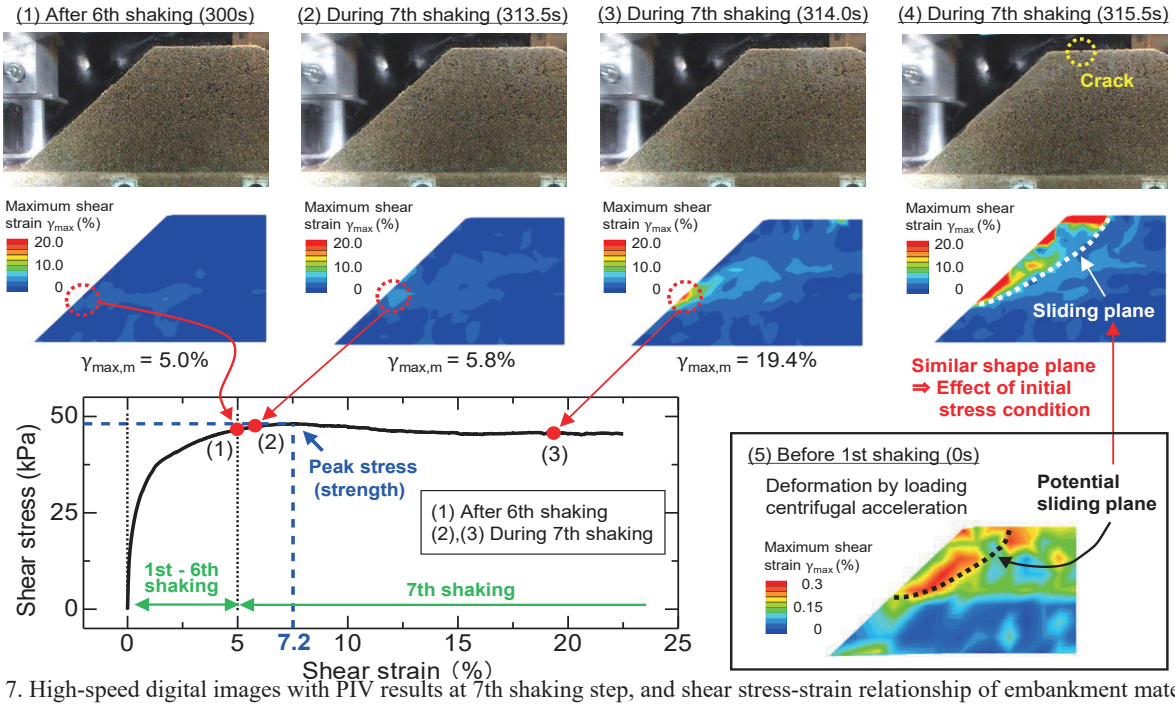

Fig. 7. High-speed digital images with PIV results at 7th shaking step, and shear stress-strain relationship of embankment material.

relatively upper part on the slope. This result is thought to be the cause of weak part at the slope created during construction process.

4 CONCLUSIONS

In this study, we investigated the damage process of an embankment during earthquakes up to sliding failure by conducting the centrifugal shaking table test. To observe deformation of embankment during earthquakes in detail, high-speed and high-resolution digital images of the embankment were taken during earthquakes in a centrifugal acceleration of 50G and the PIV analysis was employed using the digital images. As a result, the following conclusions were obtained.

1) Clear digital images without camera shake could be taken using the high-speed camera fixed to the shake table. Progress of strain inside the embankment, therefore, could be obtained from the PIV analysis using the digital images.
2) Shear strain tends to concentrate at the edge of the potential sliding plane formed before shaking and progresses into the inside of embankment along the plane during an earthquake. Finally, a sliding plane appeared and fully collapsed.
3) An embankment could show sliding failure when the shear strain at the edge of the potential sliding plane reaches the strain at the peak stress of the embankment material.

REFERENCES

Cilingir, U. & Madabhushi, S.P.G. 2011. Effect of depth on the seismic response of square tunnels. Soils and Foundations, Vol. 51, No. 3: 449-457.

Fujiwara, T., Nakamura. H., Taniguchi, Y. Takasaki, H. & Kaneda, J. 2015. A study about factors which caused railway embankment damages by circular slip analysis. Journal of Japanese Society of Civil Engineering A1, Vol. 71, No. 4: I_87-94. (in Japanese)

Itoh, K., Toyosawa, Y. & Kusakabe, O. 2009. Centrifugal modeling of rockfall events. International Journal of Physical Modeling in Geotechnics, Volume 9, Issue 2: 1-22.

Izawa, J., Doi, T. & Kojima, K. 2022. Centrifuge shaking table tests on damage level of embankments before sliding failure during earthquakes. (submitted to Soil Mechanics and Geotechnical Engineering)

Makdisi, F. I. & Seed, H. B. 1978. Simplified Procedure for Dam and Embankment Earthquake-Induced Deformations. Journal of the Geotechnical Engineering division, Vol. 104, No. GT7: 849-867.

Newmark, N. M. 1965. Effects of earthquakes on dams and embankments. Geotechnique, Vol. 15, No. 2: 139-160.

Okamura, M., Matsuo, O. & Tamoto, S. 2001. A high frame rate image acquisition system for dynamic centrifuge tests. International Journal of Physical Modeling in Geotechnics, Volume 1, Issue 1: 71-76.

Railway Technical Research Institute. 2012. The Design Standards for Railway Structures and Commentary (Seismic Design). Supervised by Ministry of Land, Infrastructure and Transportation, Maruzen. (in Japanese)

Sarma, S. K. 1975. Seismic Stability of Earth Dams and Embankments. Geotechnique, Vol. 25, No. 4: 743-761.

S. Sreng, Y. Okochi, K. Kobayashi, H. Tanaka, H. Sugiyama, T. Kusaka, H. Miki & M. Mkakino 2015. Centrifuge model tests of embankment with a new liquefaction countermeasure by ground improvement considering constraint effect. 6th International Conference on Earthquake Geotechnical Engineering.

White, D. J., Take, W. A. & Bolton, M. D. 2003. Soil deformation measurement using particle image velocimetry and photogrammetry. Geotechnique, Vol. 53, No. 7: 619-631.